EuroGeo4 Paper number 228

MECHANISTIC-EMPIRICAL DESIGN METHOD FOR UNPAVED ROADS USING GEOSYNTHETICS

Steve Perkins[1], Barry Christopher[2] & Bruce Lacina[3]

[1] *Montana State University. (e-mail: stevep@ce.montana.edu)*
[2] *Christopher Consultants. (e-mail: barryc325@aol.com)*
[3] *TenCate Geosynthetics (e-mail: b.lacina@tencate.com)*

Abstract: This paper presents a preliminary Mechanistic-Empirical (M-E) design method for unpaved roads using geosynthetics. This method is based on the test procedures and results of full scale laboratory roadway stabilization model tests. It is also based on the results of specific physical property and characterization tests on the individual materials comprising the test sections. The model tests were performed on a silt type subgrade with a California bearing ratio (CBR) of 1 percent. The reinforcement benefit was evaluated in terms of the number of 40 kN (9 kip), simulated single wheel load cycles applied to reach a specific permanent rut depth of 76 mm (3 in) in the aggregate layer surface and the Traffic Benefit Ratio (TBR), the reinforced section load cycles divided by the control load cycles required to reach this same rut depth. The test sections were instrumented to measure geosynthetic deformation and subgrade pore water pressure response. A mechanistic-empirical model for unpaved roads was developed following the principles developed for reinforced paved roads. This model incorporates material and damage (rutting) models for the base aggregate, subgrade and geosynthetic materials. The model is field calibrated against the test section results.

Comment [MSOffice1]: Steve, I'm pretty sure GTX targeted 9 kips, which works out to 40 kN, not the 80 you had indicated.

Keywords: Road, Unpaved, Geosynthetic, Reinforcement, Stabilization, Design Method.

INTRODUCTION

Geosynthetic stabilized unpaved roads are typically designed using methodologies based on not exceeding the bearing capacity of the underlying subgrade materials (Bender and Barenberg, 1978; Giroud and Noiray, 1981; Steward et al., 1977). Empirical modifications to bearing capacity theory are generally added to account for the level of traffic for which the roadway should be designed. Mechanistic-empirical pavement design methodologies have been developed and used mainly for paved roadways experiencing relatively heavy volumes of traffic. Mechanistic-empirical design has the advantage of describing the effect of traffic passes on the accumulation of permanent deformation of the roadway materials.

The purpose of this paper is to describe the development of a mechanistic-empirical design for stabilized unpaved roads, which is based on methodologies developed for reinforced paved roads (Perkins et al. 2004). The design method involves the use of a finite element response model, which contains material models for the base aggregate, subgrade and geosynthetic reinforcement materials. An empirical damage model for permanent deformation of the aggregate and subgrade materials is used to relate the vertical dynamic strain from the response model to rutting as a function of traffic passes.

Laboratory testing of the materials used in the unpaved road provided input parameters for the material models contained in the finite element response model. The design method has been calibrated by comparison of unreinforced model predictions to comparable full-scale laboratory test sections. Additional stabilized tests sections containing a layer of geosynthetic reinforcement were then compared to model predictions to assess the ability of the design model to account for the positive effects of the geosynthetic. The remainder of the paper is organized by first describing the test sections and then describing the mechanistic-empirical model and showing the predictions of the test sections.

TEST SECTIONS

Two unpaved roadway test sections were constructed and loaded. One section contained no geosynthetic. The second section contained a woven geotextile, whose material properties are described below. The test sections were constructed in the Geotesting Express pavement test box facility, which was designed and constructed for the purpose of conducting full-scale laboratory experiments on reinforced and unreinforced pavement sections meeting the requirements of specifications developed for AASHTO Subcommittee 4E as contained in Berg et al. (2000).

Materials

The materials used in the construction of the test sections included a subgrade, a base aggregate and a woven geotextile. The subgrade consisted of brown sandy silt (ML-MH). The subgrade has a standard Proctor (ASTM D698) maximum density of 15.2 kN/m^3 (97 lb/ft^3) and an optimum moisture content of 22 %. The material was placed at a water content of approximately 36 %, producing an in-place CBR of 1. Vane shear tests (ASTM D2573) on in-situ material produced an undrained cohesion of 30 kPa (620 psf). The in-situ dry density and moisture content was approximately 13.4 kN/m^3 (85 lb/ft^3) and 36 %.

The base course aggregate was a graded aggregate meeting the state of Georgia Department of Transportation specifications. The material has a maximum dry density of 22.8 kN/m^3 (145 lb/ft^3) and an optimum moisture content of 5.4 %. The material has a drained friction angle of 43 degrees. The material was placed at a moisture content of 6 % and at an average dry density of 21.4 kN/m^3 (136 lb/ft^3).

The geotextile (Mirafi HP 570) was a woven polypropylene having the material properties shown in Table 1.

Table 1. Material properties of the woven geotextile

Property	Value
T_{ult} (MD), lb/ft	4800
T_{ult} (XD), lb/ft	4800
$T_{2\%}$ (MD), lb/ft	960
$T_{2\%}$ (XD), lb/ft	1320
ψ, sec^{-1}	0.4

Comment [MSOffice2]: Is there a reason that we have chosen not to include a value (published) here?

Construction

Construction of the test sections took place in a rigid box measuring 1.8 m by 1.8 m by 1.5 m (6 ft by 6 ft by 5 ft) deep. The subgrade was constructed in eight approximately 6-inch finished lifts and compacted with a gasoline powered "jumping jack" trench compactor. The lift thickness of 6 inches was chosen to yield a uniform density in the layer without large void spaces. Thickness of each layer was measured with a standard auto-level and Philadelphia rod at five locations (i.e., at the box center and at the center of each quadrant). Once a lift was compacted, samples were taken for oven drying to determine in-place moisture content ASTM D2216). The geotextile was placed directly on top of the subgrade.

The base course aggregate was placed in two 6-inch lifts for a total thickness of 12 in. The subgrade surface and the final surface of the base were surveyed to confirm the thickness. Compaction was achieved with an 8-hp vibratory plate compactor. Layer surfaces were roughened with a rake prior to a subsequent lift placement in order to facilitate layer bonding.

Loading

A cyclic load is provided to the test section by a pneumatic load actuator supported by I-beams connected to the top of the box. The actuator has a stroke of 3 inches. A 2-inch diameter steel rod extends from the actuator to a load plate, which rests on the upper pavement surface. The load plate is a 12-inch diameter plate with a thickness of 1-inch. A ¼ inch thick waffled butyl rubber pad is placed beneath the load plate in order to provide a uniform pressure and avoid stress concentrations along the plate's perimeter.

A binary solenoid regulator, attached to a computer, controlled the load-time history applied to the plate. The software controlling the solenoid is the same software used to collect data from the pavement sensors. The software is set up to provide a linear load increase from zero to 40 kN (9 kips) over a 0.3 second rise time, followed by a 0.2 second period where the load is held constant, followed by a load decrease to zero over a 0.3 second period and finally followed by a 0.5 second period of zero load before the load cycle is repeated, resulting in a load pulse frequency of 0.67 Hz. The maximum applied load of 40 kN (9 kips) resulted in a pavement pressure of 550 kPa (80 psi). This load represents one-half of an axle load from an equivalent single axle load (ESAL). The load frequency is selected to allow the data acquisition system time to store data before the next load pulse was applied.

In test sections where significant deformation (more than 1 inch) occurred during the initial load cycles, the full load could not be maintained (with a measured drop off of up to 20%). Periodic adjustments were required during the tests. The modeling process accounted for this by analyzing mechanistic response models subjected to various load plate pressures.

Load cycles were applied until a permanent surface deformation below the plate of at least 76 mm (3 in) was reached or a minimum of 10,000 applied loads, whichever occurred first. In most cases after the required rutting had occurred the rut was filled in with aggregate (i.e., brought back to the original grade) and the test was repeated.

Instrumentation

Instrumentation was included in the test sections. The instrumentation is designed to be utilized to evaluate rutting in the stabilization aggregate and pore water pressure response of the subgrade during placement, compaction and subsequent loading. Instrumentation was included to make the following measurements:

- Vertical surface deformation in the stabilization aggregate layer
- Applied load to the plate
- Pore pressure in the subgrade during construction and pavement loading

Results

Figure 1 shows results of the peak pressure on the load plate for each cycle of the control test and the test with the geotextile. The data illustrates the difficulty with holding the load constant as discussed above. Figure 2 shows the results of the permanent surface deformation plotted against load cycle. Figure 3 shows results of the dynamic deformation plotted against load cycle. Figure 4 shows the excess pore pressure in the top of the subgrade versus load cycle for the unreinforced (control) and the geosynthetic test sections, where it is seen that significantly more pore water pressure builds up in the unreinforced test section.

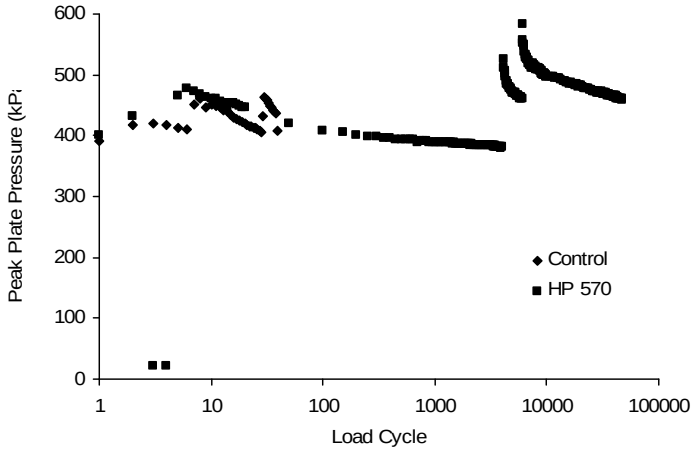

Figure 1. Peak load plate pressure versus load cycle

Comment [MSOffice3]: I hate to say it at this late date, but, triangles might be more easily discerned from squares than diamond shapes where the data overly each other for the 2 tests…

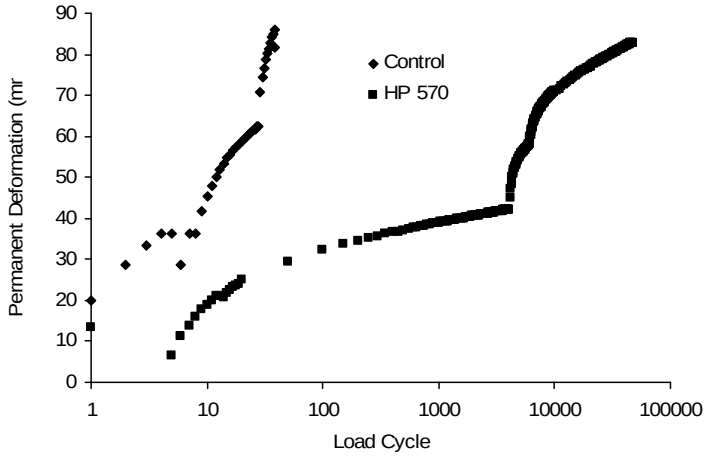

Figure 2. Permanent surface deformation versus load cycle

Comment [MSOffice4]: We seem to be loosing the end of the y-axis titles on these plots. Is that something that is easily remedied?

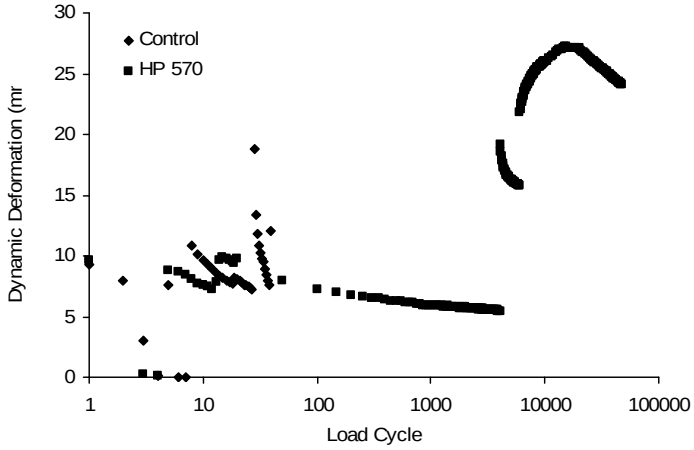

Figure 3. Dynamic deformation versus load cycle

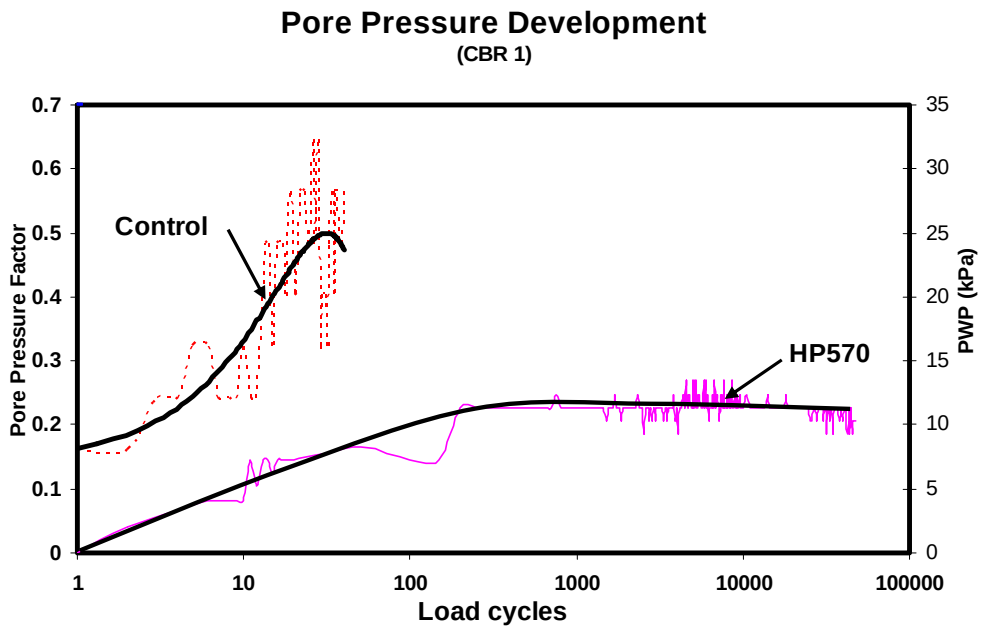

Figure 4. Excess pore-pressure in the subgrade versus load cycles

MECHANISTIC-EMPIRICAL MODEL

The mechanistic-empirical modeling process involved in this project encompasses the following basic steps:

- Creation of an unreinforced finite element model and determination of the vertical dynamic strain under the load-plate centerline as a function of depth in the base aggregate and subgrade layers.
- Adjustment of the subgrade resilient modulus in the unreinforced finite element model to reflect the reduction in modulus due to pore-water pressure build-up in the corresponding test section and to match the dynamic surface deflection seen in the test section.
- Prediction of rutting versus applied load cycles for the unreinforced test section using an empirical damage model for rutting and the dynamic vertical strain distribution obtained in step 1.
- Field calibration of the damage model for rutting by optimization of the damage model parameters.
- Creation of a reinforced finite element model accounting for the effects of compaction and traffic-induced horizontal stress confinement in the aggregate layer.
- Determination of the vertical dynamic strain under the load-plate centerline as a function of depth in the base aggregate and subgrade layers for the reinforced model.
- Prediction of rutting versus applied load cycles for the reinforced test section using an empirical damage model for rutting and the dynamic vertical strain distribution obtained in the step above.
- Comparison of the predicted rutting to the rutting observed in the test section.

The following sections describe these steps in more detail.

Response model input

Finite element response models were created to match the geometry of the unreinforced and reinforced test sections. The models were axisymmetric models with a radius of 1.12 m (3.67 ft), which was chosen to give the same plan area as the test section box. The models were created with a base aggregate and a subgrade layer. The base aggregate layer was 0.30 m (12.0 in) in thickness and the subgrade was 1.22 m (4.0 ft) in thickness for both the unreinforced and reinforced models. The models were meshed following the same guidelines as described in Perkins et al. (2004). The reinforced section contained a membrane sheet representing the reinforcement, which was placed between the base aggregate and the subgrade. Interface contact surfaces were created between the reinforcement and the surrounding base aggregate and subgrade layers.

A non-linear elastic material model was used for the base aggregate layer. The resilient modulus of the material is described by Equation 1, where the material properties were determined from resilient modulus tests.

(Eq. 1)

M_R = resilient modulus
p_a = atmospheric pressure (101.3 kPa)
θ = bulk stress
τ_{oct} = octahedral shear stress
k_1 = 842
k_2 = 0.6476
k_3 = -0.01511

A linear elastic model was used for the subgrade. Resilient modulus and permanent deformation testing on the subgrade material showed that the subgrade has an elastic modulus between 5.5 to 6.9 MPa (800 to 1000 psi). The use of a modulus of 6 MPa (870 psi) in the finite element model for the unreinforced test section resulted in an overly stiff response with a dynamic deflection that was less than the observed average value of approximately 8 mm (0.31 in). The pore-water pressure build-up in the subgrade layer of the unreinforced test section results in a reduction of both strength and stiffness of the subgrade. After construction, the subgrade has an undrained shear strength of 30 kPa (4.4 psi) as measured from a vane shear test. In the unreinforced test section, the excess pore water pressure is seen to increase by an average value of approximately 21 kPa (3.0 psi). This reduces the effective stresses in the material and results in a lower value of undrained shear strength and stiffness. If an effective strength friction angle of 30 degrees is assumed, then it can be shown that an increase in pore water pressure of 21 kPa results in an undrained shear strength of 9.3 kPa (1.3 psi). If the decrease in undrained shear strength is assumed to be proportional to the decrease in elastic modulus, then the material will have a new modulus of 1860 kPa (270 psi). The use of this modulus in the unreinforced response model resulted in a dynamic deflection that matched the observed value of approximately 8 mm.

For the reinforced test section, the excess pore water pressure was approximately 7 kPa (1.0 psi). Using the same approach described above, the elastic modulus of the subgrade for the reinforced test section was 4600 kPa (667 psi). Following guidelines established by Perkins et al. (2004), the cyclic elastic modulus of the geotextile in the machine and cross-machine directions and the material's Poisson's ratio was used to determine an equivalent isotropic elastic modulus of 791,476 kPa (115 ksi).

Reinforced response model modules corresponding to compaction, traffic 1, traffic 2 and traffic 3 modules were created, where these modules were described by Perkins et al. (2004). The compaction module describes the increase in lateral confining stress in the base aggregate during the compaction of the aggregate. The traffic 1, 2 and 3 modules are used to define the build-up of lateral stress in the aggregate during traffic loading of the section.

In the unreinforced and reinforced test sections, the applied pavement load was seen to vary as illustrated in Figure 1. This led to several approaches to model this load variation in the response models. For the case of the unreinforced model, a series of analyses were made with the load plate pressure varying according to that observed in the test section. This was compared to an analysis using the average load plate pressure. Results from this comparison are illustrated in Figure 5.

From the unreinforced and reinforced response models, the distribution of dynamic vertical strain with depth through the base aggregate and subgrade layers was determined and used in a damage model for rutting, as described in the next section.

Rutting model and input

A damage model for rutting was used for the base aggregate and subgrade layers to predict rutting versus applied load. The equation for the model is given by Equation 2

$$\varepsilon_p = \varepsilon_r \, \xi_1 A e^{-\left(\frac{\rho}{N}\right)^{\xi_2 B}} \qquad \text{(Eq. 2)}$$

where ε_p is the permanent strain and ε_r is the resilient or dynamic strain determined from the response model, A, B and ρ are material properties, and ξ_1 and ξ_2 are field calibration parameters.

The material properties were determined from permanent deformation tests on each material. The field calibration values were determined by comparison and optimization of predicted versus measured rutting in the unreinforced test section. Table 2 presents the parameters contained in Equation 2 for the base aggregate and subgrade soils.

Table 2. Permanent deformation model parameters for unbound materials

	ρ	A	B	ξ_1	ξ_2
Aggregate	2140	90	0.45	1.00	0.400
Subgrade	4.56+20	1410	0.037	1.00	1.02

Calibration against unreinforced test section

The unreinforced model was analyzed by first evaluating the dynamic surface deflection and comparing it to the observed average value of approximately 8 mm (0.31 in) seen in the test section. This, along with the analysis of the effects of excess pore water pressure, resulted in the use of a subgrade resilient modulus of 1860 kPa (270 psi).

The unreinforced model was then analyzed using the history of load plate pressure versus applied cycles from the test section. This was done by analyzing the unreinforced finite element model for each of the load plate pressure values recorded during the pavement load test. The dynamic vertical strain distribution from each analysis was then used in the damage rutting model to determine the permanent surface deformation after each unique applied load. The results of this analysis are shown in Figure 5 and are compared to the results from the test section.

In the test section, the load actuator was adjusted at cycle 28 and the load plate pressure jumped from approximately 406 kPa to 460 kPa (59 psi to 67 psi) with the rutting accelerating as seen in Figure 5. The prediction using the actual load history was unable to show this jump in rutting. The rutting model is not well-suited for accounting for an increase in pavement load for a system that ruts appreciably over a relatively small number of cycles.

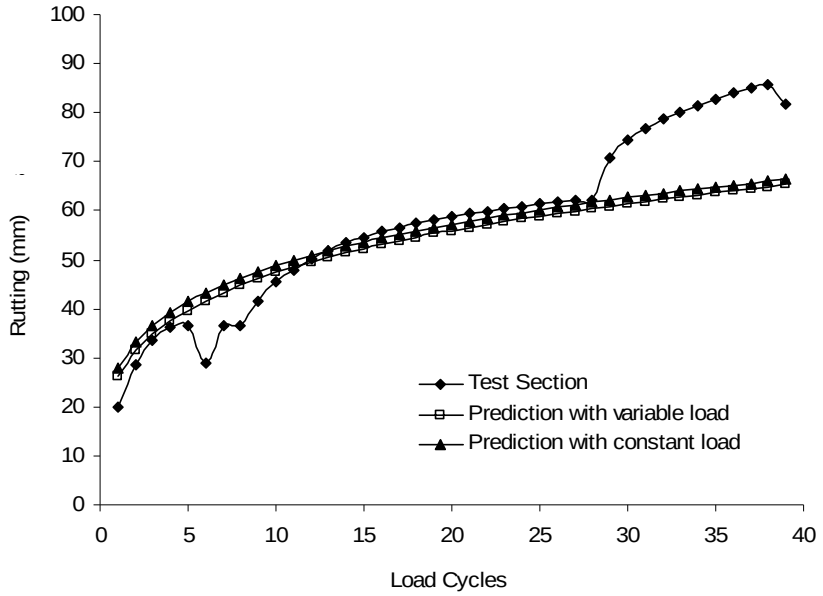

Figure 5. Unreinforced rutting predictions compared to test section results

A second analysis was performed using a constant pavement load of 420 kPa (61 psi), which was an average value for the first 39 cycles. The results of this analysis are shown in Figure 5 and are seen to be very close to the analysis using the actual loading history.

The predictions of the unreinforced section show good agreement to the test section results when the load plate pressure is relatively constant. The field calibration factors used in this analysis (Table 2) are well within a reasonable range and indicate that the models employed in this analysis are well-suited for the application.

Comparison to reinforced test section

The reinforced response model modules used a resilient modulus for the subgrade of 4600 kPa (667 psi) to account for the smaller increase in excess pore water pressure seen in the reinforced test section. The reinforced response model modules accounted for the following conditions, where the modeling steps associated with these conditions were described by Perkins et al. (2004):

- Build-up of horizontal stress during aggregate layer compaction
- Build-up of horizontal stress during traffic loading
- Reduction in permanent deformation properties of the reinforced aggregate layer

To assess the effect of the increase in subgrade modulus due to the smaller increase in excess pore water pressure, a series of analyses were performed using the reinforced and unreinforced models. The following analyses were performed and are illustrated in Figure 6.

- An unreinforced model with a subgrade modulus of 1860 kPa (270 psi) and a load plate pressure of 420 kPa (61 psi).
- An unreinforced model with a subgrade modulus of 4600 kPa (667 psi) and a load plate pressure of 420 kPa.
- An unreinforced model with a subgrade modulus of 4600 kPa and a load plate pressure of 385 kPa (56 psi).
- A reinforced model with a subgrade modulus of 4600 kPa and a load plate pressure of 385 kPa.

Analyses 1 and 2 allow for an assessment of the effect of increasing the subgrade modulus. Analyses 3 and 4 allow for an assessment of the additional effect of modeling the reinforcement. The results show that at a 1000 load cycles, the effect of increasing the modulus to account for lower excess pore water pressure is to reduce the rutting by approximately 50 mm (2.0 in). An additional 13 mm (0.5 in) of rutting reduction is seen by accounting for the effects of the reinforcement.

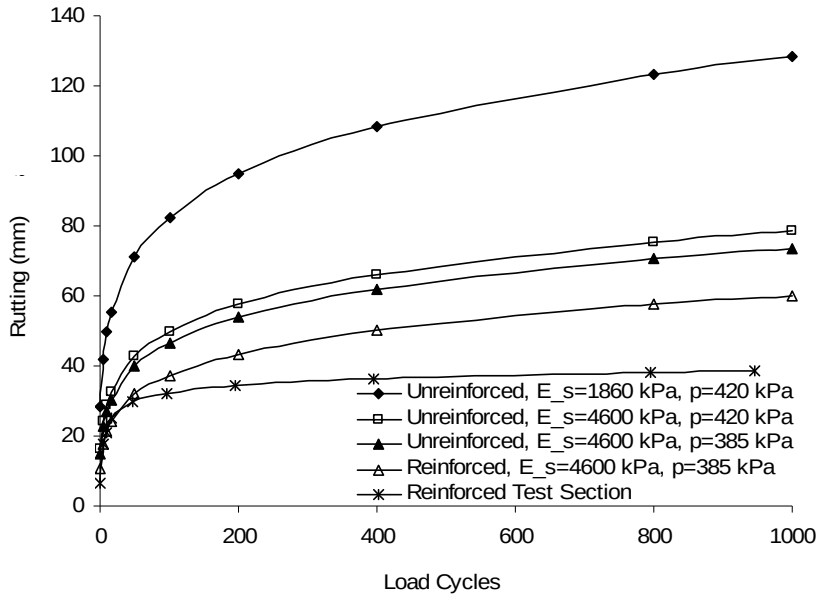

Figure 6. Reinforced rutting predictions and comparisons

CONCLUSION

Mechanistic-empirical modeling of the unsurfaced pavement test sections has shown good agreement with the unreinforced test, with the exception of showing the accelerated rutting seen when the load plate actuator was adjusted and the change in applied pressure increased. The steps taken to account for the reduced excess pore water pressure in the reinforced test section as compared to the unreinforced section accounts for approximately 80 % of the reduced rutting. An additional 20 % is accounted for by modeling the effects of the reinforcement. Overall, the prediction of rutting using the reinforced model is greater than that seen in the reinforced test section but shows considerable improvement as compared to the unreinforced section and is regarded as a favorable and successful prediction.

Acknowledgements: The financial support of TenCate Geosynthetics for the performance of this study is gratefully acknowledged. Geotesting Express is acknowledged for their performance of the testing program, Geocomp Corporation for their contribution to the instrumentation of the test section, and the Georgia Department of Transportation for providing the soil used in this study. Special thanks go to Dr. Allen Marr for his input in the interpretation of the test section data and Mr. Jianren Wang and Mr. Marty Molino for their oversight and technical contributions during the testing program.

Corresponding author: Dr Steve Perkins, Montana State University, 205 Cobleigh Hall, Bozeman, Montana, 59717, United States of America. Tel: 1-406-994-6119. Email: stevep@ce.montana.edu.

REFERENCES

Bender, D.A. and Barenberg, E.J. 1978. Design and Behavior of Soil-Fabric-Aggregate Systems, Transportation Research Record No. 671, pp. 64-75.

Berg, R.B., Christopher, B. R. and Perkins, S. 2000. Geosynthetic Reinforcement of the Aggregate Base/Subbase Courses of Pavement Structures, prepared for American Association of Highway and Transportation Officials Committee 4E, Prepared by the Geosynthetic Materials Association, 2000, 176 p.

Giroud, J.-P. and Noiray, L. 1981. Geotextile-Reinforced Unpaved Road Design, Journal of Geotechnical Engineering, ASCE, Vol. 107, No. GT9, pp. 1233-1254.

Perkins, S.W., Christopher, B.R., Cuelho, E.L., Eiksund, G.R., Hoff, I., Schwartz, C.W., Svanø, G., and Watn, A. 2004. Development of Design Methods for Geosynthetic Reinforced Flexible Pavements, U.S. Department of Transportation, Federal Highway Administration, Washington, DC, FHWA Report Reference Number DTFH61-01-X-00068, 263p.

Steward, J.E., Williamson, R. and Mohney, J. 1977. Guidelines for Use of Fabrics in Construction of Low-Volume Roads, Report No. FHWA-TS-78-205, Pacific Northwest Region Forest Service, U.S. Department of Agriculture, Washington, DC, USA, 172p.